Redox Biology 22 (2019) 101158

Contents lists available at ScienceDirect

Redox Biology

journal homepage: www.elsevier.com/locate/redox

Role of nitric oxide in pancreatic cancer cells exhibiting the invasive phenotype

Mayumi Fujita[a,b,*], Veena Somasundaram[a], Debashree Basudhar[a], Robert Y.S. Cheng[a], Lisa A. Ridnour[a], Harumi Higuchi[b], Kaori Imadome[b], Jae Hong No[a,c], Gaurav Bharadwaj[a], David A. Wink[a,**]

[a] Cancer and Inflammation Program, Center for Cancer Research, National Cancer Institute, National Institutes of Health, MD, USA
[b] Department of Basic Medical Sciences for Radiation Damages, National Institute of Radiological Sciences, National Institutes for Quantum and Radiological Science and Technology, Chiba, Japan
[c] Department of Obstetrics and Gynecology, Seoul National University Bundang Hospital, Seongnam, Republic of Korea

ARTICLE INFO

Keywords:
Nitric oxide
Nitric oxide synthase
Pancreatic cancer
Invasion
Metastasis
Cancer stem cell

ABSTRACT

Pancreatic cancer is a highly metastatic tumor with an extremely low 5-year survival rate. Lack of efficient diagnostics and dearth of effective therapeutics that can target the cancer as well as the microenvironment niche are the reasons for limited success in treatment and management of this disease. Cell invasion through extracellular matrix (ECM) involves the complex regulation of adhesion to and detachment from ECM and its understanding is critical to metastatic potential of pancreatic cancer. To understand the characteristics of these cancer cells and their ability to metastasize, we compared human pancreatic cancer cell line, PANC-1 and its invading phenotype (INV) collected from transwell inserts. The invasive cell type, INV, exhibited higher resistance to Carbon-ion radiation compared to whole cultured (normally dish-cultured) PANC-1 (WCC), and had more efficient *in vitro* spheroid formation capability. Invasiveness of INV was hampered by nitric oxide synthase (NOS) inhibitors, suggesting that nitric oxide (NO) plays a cardinal role in PANC-1 invasion. In addition, *in vitro* studies indicated that a MEK-ERK-dependent, JAK independent mechanism through which NOS/NO modulate PANC-1 invasiveness. Suspended INV showed enhanced NO production as well as induction of several pro-metastatic, and stemness-related genes. NOS inhibitor, L-NAME, reduced the expression of these pro-metastatic or stemness-related genes, and dampened spheroid formation ability, suggesting that NO can potentially influence pancreatic cancer aggressiveness. Furthermore, xenograft studies with INV and WCC in NSG mouse model revealed a greater ability of INV compared to WCC, to metastasize to the liver and L-NAME diminished the metastatic lesions in mice injected with INV. Overall, data suggest that NO is a key player associated with resistance to radiation and metastasis of pancreatic cancer; and inhibition of NOS demonstrates therapeutic potential as observed in the animal model by specifically targeting the metastatic cells that harbor stem-like features and are potentially responsible for relapse.

1. Introduction

Pancreatic cancer is a highly metastatic tumor with an extremely low 5-year survival rate [1–3]. During metastasis, cancer cells undergo a multi-step process where they invade through the tumor tissue and the basal membrane into a blood or lymphatic vessel [4]. Once tumor cells are in the circulatory system, they can reach and reattach to favorable niches in different organs followed by colonization. Metastasis is the main cause of patient mortality as it is extremely difficult to treat. Understanding the characteristics of the cancer cell population that exhibits the invasive phenotype compared to the non-invasive phenotype is fundamental for developing novel strategies to counter metastasis.

Carbon ion radiation therapy (C-ion RT) has emerged as an important therapeutic option specially for advanced, inoperable pancreatic cancers. It can provide a highly conformal dose distribution so

* Corresponding author. Department of Basic Medical Sciences for Radiation Damages, National Institutes for Quantum and Radiological Science and Technology, 4-9-1, Anagawa, Inage-ku, Chiba-shi, Chiba-ken, 263-8555, Japan.
** Corresponding author. Cancer and Inflammation Program, National Cancer Institute, Bldg. 567 Rm 254, 1050 Boyles St., Frederick, MD 21702, USA,
E-mail addresses: fujita.mayumi@qst.go.jp (M. Fujita), wink@mail.nih.gov (D.A. Wink).

https://doi.org/10.1016/j.redox.2019.101158
Received 30 January 2019; Received in revised form 28 February 2019; Accepted 1 March 2019
Available online 06 March 2019

Abbreviations

C-ion RT	carbon ion radiation therapy
CSC	cancer stem-like cells
DAF-FM	4-amino-5-methylamino-2′,7′-difluorofluorescein diacetate
ECM	extracellular membrane
EMT	epithelial-mesenchymal transition
ERK	extracellular signal-regulated kinase
INV	invaded PANC-1 cells
INVS	INV suspended in serum free media for 4 h
JAK	janus kinase
L-NAME	N(G)-nitro-L-arginine methyl ester
L-NMMA	N(G)-monomethyl-L-arginine, monoacetate salt
MMP9	matrix metallopeptidase 9
NO	nitric oxide
NO_2^-	nitrite
NO-sGC pathway	soluble guanylyl cyclase pathway
NOS	nitric oxide synthase
NSG mice	NOD scid gamma mice
ODQ	1H-[1,2, 4]oxadiazolo[4,3,-a]quinoxalin-1-one
P-ERK	phosphorylated-ERK
P-MEK	phosphorylated-MAPK/ERK kinase
STAT	signal transducers and activators of transcription
WCC	whole cultured PANC-1 cells
WCC_S	WCC suspended in serum free media for 4 h

that a high dose can be delivered to tumors with minimum damage to the surrounding healthy tissue [5]. Recent studies showed that C-ion RT led to favorable outcomes both as a stand-alone therapy as well as in combination with gemcitabine, a chemotherapeutic used for pancreatic cancer. Moreover, the therapy was well-tolerated with limited toxicities [6,7]. The merit of C-ion RT is further substantiated by a clinical trial that was initiated last year [8]. However, it is also known that some malignant tumors exhibit resistance to radiotherapy [9]. Our previous study indicated that invasive cells may exhibit a stable and distinguishable phenotype that may impart special, therapy resistant characteristics to these cells [10,11]. Therefore, it is crucial to establish whether pancreatic cancer shows phenotype dependent resistance to C-ion RT and examine their mechanism of resistance.

Development of relevant *in vitro* and *in vivo* models is a key step in understanding phenotypic differences in the response to C-ion RT. The Boyden chamber transwell assay is a widely used experimental method for studying tumor cell invasiveness *in vitro* [12]. Several studies on pancreatic cancer cells have shown that only a very small percentage of the cells could invade through the transwell in pancreatic cancer cell lines studied [10,13–15]. In the case of PANC-1 cells, we have previously found that only about one percent of seeded cells invaded through the transwell [15]. This was further investigated using a 3D spheroid model of PANC-1, embedded in Matrigel, coupled with live cell imaging analysis to capture the movement of the distinct invading population [11]. These invaded PANC-1 cells (INV) exhibited increased nitric oxide (NO) production compared to whole cultured PANC-1 cells (WCC) and, the nitric oxide synthase (NOS) inhibitor, N^G-monomethyl-L-arginine, monoacetate salt (L-NMMA), was effective in reducing PANC-1 invasion [15]. INV and WCC cells that are both collected from PANC-1 parental cell line, are isogenic yet express distinctive phenotypes. Hence, in this study, we use the WCC as the control group for comparison with the INV cells that have invaded through the transwell chamber.

Herein, we establish that invasive cell phenotype that leads to the metastatic spread of pancreatic cancer is a discernible and persistent phenotype that is resistant to C-ion radiation. This phenotype showed upregulation of NO production and was effectively targeted using a pan-NOS inhibitor for improved therapy response in NSG mouse model for pancreatic adenocarcinoma metastasis. *In vitro* studies point towards a MEK-ERK-dependent, JAK signaling independent mechanism through which NOS/NO modulate invasiveness in PANC-1. Our results convincingly establish that inhibition of NO production is a viable therapeutic option to improve efficacy of C-ion RT.

2. Materials and methods

2.1. Cell culture and reagents

The human pancreatic cancer cell line, PANC-1 was purchased from ATCC (Manassas, VA, USA) and cultured in Dulbecco's modified Eagle's medium (DMEM; Gibco, Gaithersburg, MD, USA) supplemented with 10% fetal bovine serum (FBS, Atlanta Biologicals, GA, USA), 2 mM L-glutamine, and 100 U/ml penicillin/streptomycin (Gibco) in a humidified atmosphere with 5% CO_2 at 37 °C. Cells in logarithmic growth phase seeded at an appropriate density were used for all experiments. 1400W-HCl (Wako, Osaka, Japan), 1H-[1,2, 4]oxadiazolo[4,3,-a]quinoxalin-1-one (ODQ) (Thermo Fisher Scientific, Burlington, MA, USA), N(G)-Nitro-L-arginine methyl ester (L-NAME) (Sigma-Aldrich, St. Louis, MO, USA), U0126 (Millipore, Billerica, MA, USA), InSolution ERK inhibitor II (Millipore), JAK Inhibitor I (Millipore) were the inhibitors used.

2.2. INV preparation and re-invasion assay

To prepare the invaded cells, transwell invasion assays were performed as described previously [11]. Briefly, cells were trypsinized and viable cell numbers were counted with trypan blue and separated into two groups; one of them was for the whole cultured cells (WCC), the other set was for preparing the invaded cells (INV). For WCC, cells were suspended in DMEM with 10% FBS, and plated on the culture dish at the appropriate density. For preparation of INV, cells were suspended into serum-free DMEM, and 1 × 10^6 cells were seeded into upper well of each transwell chambers (the 24 mm transwell insert diameter with a pore size of 8 μm, Corning) coated with 260 μL Matrigel (2.9 mg/mL concentration). DMEM supplemented with 10% FBS was added to the lower well as a chemoattractant. After 24 h, the non-invasive cells remaining on the Matrigel-coated side were wiped off with a cotton swab, and the cells that moved through to the undersurface of the transwell membrane were collected by incubating the cells with Accutase (Innovative Cell Technologies, San Diego, CA, USA) for 15 min at room temperature. INV collected from several transwells were pooled, suspended in DMEM with 10% FBS and plated on the culture dish at the appropriate density. For the re-invasion assay, WCC and INV were trypsinized on day 1, 4, 7, 11, or 18 after cultivation, and the transwell invasion assay was repeated with these cells (Supplemental Fig. 1).

2.3. Transwell invasion assay

The invasive potential of PANC-1 cells was examined as previously described [15]. Briefly, matrigel was added to culture insert of transwell chambers containing a 6.5-mm filter with a pore size of 8 μm (Corning, NY, USA), and 1.5 × 10^5 cells suspended with serum-free DMEM were seeded onto it. DMEM with 10% FBS was added to the lower well, and the invasion assay was performed for 24 h. Invasive cells that reached the undersurface of the transwell membrane were fixed and stained with Diff Quick (Sysmex, Kobe, Japan). The transwell membrane were photographed and number of invaded cells in each field were counted with ImageJ software. Percentage of invaded cells was calculated by dividing the number of invaded cells with the number of seeded cells on the transwell membrane.

For inhibitor studies, cells were pre-treated with 1400W, ODQ, L-NAME, U0126, ERK inhibitor II or JAK inhibitor I, and incubated for 16 h. Cells were then trypsinized, suspended in serum-free DMEM with appropriate inhibitor, and used for the invasion assay.

2.4. Irradiation and colony formation assay

Cells were irradiated with either X-ray or Carbon ion (C-ion) radiation and the colony formation assay was performed as previously described [16,17]. Briefly, cells were irradiated with the C-ion radiation with initial energy of 290 MeV/u and the linear energy transfer value as 80 keV/μm corresponding to a mono-energetic beam with narrow Bragg Peak at a depth of 10 cm. X-ray irradiation was performed as described previously [17]. Cells were then trypsinized and plated in 60-mm diameter plastic dishes and cultured for 13 days. Colonies were then fixed and stained with 1% methylene blue in 30% methanol, and those consisting of > 50 cells were scored as a surviving colony.

2.5. NOS inhibitor treatment and suspension of cells

PANC-1 cells were plated in DMEM with 10% FBS. After 24 h, culture medium was changed to serum-free DMEM with or without NOS inhibitors and cells were incubated for 16 h. For the suspended cell group, cells were then trypsinized and suspended for 4 h in serum-free DMEM with or without NOS inhibitors, and used for DAF-FM staining, and RNA or protein sampling. For the adherent cell group, cells were directly used for the experiments.

2.6. Detection of NO producing cells

DAF-FM (4-Amino-5-Methylamino-2′,7′-Difluorofluorescein Diacetate) (Thermo Fisher Scientific, Waltham, MA, USA) [18] was used for the detection of NO-producing cells according to the manufacturer's protocol. Briefly, cells were washed twice with PBS, followed by staining with DAF-FM in serum-free DMEM for 45min. Cells were then washed with PBS and three randomly selected fields were imaged with a fluorescence microscope. Percentage of NO-producing cells was calculated by dividing the number of DAF-FM-positive cells with the total number of cells visualized in bright field image. For the prolonged detection of DAF-FM signals, 1 × 10^4 cells, which were suspended in serum free DMEM, were plated on black 96 well plate, and fluorescent signals were detected every 30 min for 17 h using the SpectraMax microplate reader (Molecular Devices, San Jose, CA, USA).

2.7. RNA extraction and RT-PCR

Total RNA was extracted with TRizol (Invitrogen) according to the manufacturer's protocol. RNA samples were reverse transcribed into cDNA using RNA to cDNA EcoDry Premix (TAKARA, Kusatsu, Shiga, Japan) according to the manufacturer's protocol. Primer sequences used in this study are summarized in Table 1. RT-PCR reactions were designed to follow a universal real time PCR condition: 94 °C for 2 min, 45 cycles at 94 °C for 30 s each, and 60 °C for 30 s in the SensiFAST Syber Lo-ROX master mix (Bioline, London, UK). Relative expression of mRNA was calculated using the ddCt formula.

2.8. Capillary western blot

Western blots were performed using WES according to the manufacturer's protocol (ProteinSimple, San Jose, CA, USA) [19]. Briefly, cells were directly lysed on ice with lysis buffer (Cell Signaling Technology, Danvers, MA, USA), sonicated, and supernatant was collected. Protein concentration was measured with BCA protein assay (Thermo Fisher Scientific, Burlington, MA, USA). Protein samples (2 μg), blocking reagent, wash buffer, primary antibodies, secondary antibodies, and chemiluminescent substrate were prepared and dispensed into the assay plate. Assay plate was then loaded into the instrument, and protein was separated into individual capillaries. Protein separation and detection was performed automatically on the individual capillaries. For the primary antibodies, p-eNOS ser1177 (Cell Signaling Technology, Danvers, MA, USA) and HPRT (Santa Cruz Biotechnology, Santa Cruz, CA, USA) were used with anti-mouse or anti-rabbit secondary antibodies provided by ProteinSimple.

2.9. Spheroid formation assay

Spheroid formation assay was performed in ultra-low attachment round bottom 96 well plates (Nexcelom, Lawrence, MA, USA) [20]. Cells (1 × 10^3) were plated in each well with serum-free DMEM supplemented with 20 ng/mL bFGF and B-27 (1:50) with or without DETA/NO or L-NAME and incubated in CO_2 incubator. Media was supplemented on day 4. Image of spheroid was captured, and diameter of spheroid was measured with Celigo Imaging Cytometer (Nexcelom) on day 9 after seeding the cells for spheroid formation.

2.10. Immunofluorescence labeling and image acquisition

Immunofluorescence labeling, and image acquisition was performed as described previously with some modifications [15]. Briefly, cells were fixed with 4% paraformaldehyde in phosphate-buffered saline (PBS; Nissui Pharmaceutical Co., Ltd.; Tokyo, Japan) for 15 min, washed with PBS, and suspended in ice-cold methanol for 10 min at −20 °C. Cells were then blocked with PBS containing 5% fetal calf serum and 0.3% Triton X100, followed by incubation with primary antibody for overnight at 4 °C. The primary antibodies against P-MEK (Cell Signaling Technology) and P-ERK (Cell Signaling Technology) were suspended in PBS containing 1% FCS and 0.3% Triton X100 at 1:100 dilution and used for the assay. Cells were then treated with AlexaFluor 555- or AlexaFluor 488-labeled anti-mouse IgG or anti-rabbit IgG secondary antibodies (Invitrogen, Carlsbad, USA) for 1 h at room temperature. The slides were mounted with ProLong Gold Antifade Reagent containing the nuclear counterstain DAPI (Invitrogen). Fluorescent signal was visualized and photographed with a BZ-9000

Table 1
Primer table.

Gene Name	Direction	Primer Sequence
NOS1	F	GGAATCCAGGTGGACAGAGA
	R	TTCCCCCATAGGTCATTGAA
NOS2	F	ATGCTCAGCTCATCCGCTAT
	R	CGATGCACAGCTGAGTGAAT
NOS3	F	GATGCTCCCAACTTGACCAT
	R	TAGGTCTTGGGGTTGTCAGG
MMP9	F	CATCGTCATCCAGTTTGGTG
	R	AGGGACCACAACTCGTCATC
S100A8	F	TCAGGAAAAAGGGTGCAGAC
	R	ACGCCCATCTTTATCACCAG
5-LOX	F	CAAAGCGATGGAGAACCTGT
	R	TTTCTCAAAGTCGGCGAAGT
CXCR4	F	CGTCTCAGTGCCCTTTTGTT
	R	CTCTCCTCCCCATCTTTTCC
CDH1	F	GGTTCAAGCTGCTGACCTTC
	R	TTGTACGTGGTGGGATTGAA
CD133	F	CCTCATGGTTGGAGTTGGAT
	R	TTCCACATTTGCACCAAAGA
ALDH1	F	CTCAAGGCCCTCAGATTGAC
	R	GTTTGGCCCCTTCTTTCTTC
NANOG	F	ACAGGTGAAGACCTGGTTCC
	R	CTGGGGTAGGTAGGTGCTGA
SOX2	F	AACTCACCAGGATGCTCACA
	R	GCACTTCCTCCAGAGGTTTG
ACTB	F	GCAAGGCCGGCTTCGCGGGC
	R	TCACGCCCTGGTGCCTGGGGC
RPL18	F	GGATGATCCGGAAGATGAAG
	R	CCGCACATCATCAGTTATGG

fluorescence microscope (Keyence, Osaka, Japan) using a 20× Plan fluorescence lens (N.A 0.45) with BZ filters for Texas Red, GFP, and DAPI. Representative images were uniformly processed in Adobe Photoshop using the brightness and contrast tools.

To count the number of P-MEK or P-ERK high, intermediate or low expressing cells, we analyzed the images with the Image J software program (Supplemental Fig. 2 for P-MEK and Supplemental Fig. 3 for P-ERK). We first used DAPI images and counted the number of cell nuclei per image, which represents the total number of cells per image. Next, the anti-P-MEK or anti-P-ERK antibody-stained images were converted into 8-bit grayscale images. The thresholding tool of the Image J software program, which can separate the pixels that fall within a desired range of intensity values from those which do not, was used to separate the cells with low, intermediate, or high accumulation of P-MEK or P-ERK. The criteria for the cells containing low, intermediate, or high ubiquitylated proteins accumulation were stated in figure legends. The number of cells ranged from 19 to 86 per group.

2.11. In vivo metastasis model

The Animal Care and Use Committee (National Cancer Institute, NIH, Bethesda, MD) approved the protocols. Male NOD scid gamma mice (NSG mice) were supplied by the National Institutes of Health, USA. Mice were received at 5 weeks of age, housed five per cage, and given autoclaved food and water *ad libitum*. Experiments were performed at 7 weeks of age in accordance with the Guide for the Care and Use of Laboratory Animals (Institute of Laboratory Animal Resources, National Research Council, Washington, DC). WCC and INV suspended in PBS with 2% Matrigel were prepared and 2 × 10^5 cells/100 μL were injected into the spleens of anesthetized mice. Designated groups of animals were treated with L-NAME in the drinking water at a concentration of 0.5 g/L for the duration of the experiment [21]. On day 25, mice were euthanized, and spleen, liver and lung were harvested. Spleen and liver were weighed immediately after the harvest, and liver and lung were fixed with Bouin's solution. Forty-eight hours later, liver and lung were washed thrice with 70% ethanol and placed in 70% ethanol solution for 48 h. Metastatic colonies were counted under stereoscopic microscope.

2.12. Statistical analysis

All results are expressed as the mean ± SD. Statistical analyses were performed using unpaired Student's *t*-test or ANOVA. *P* value of < 0.05 was considered significant.

3. Results

3.1. Invaded pancreatic cancer cells are associated with increased invasiveness and resistance to C-ion radiation

To investigate the effect of C-ion radiation on metastatic pancreatic cancer, the classical Boyden chamber invasion assay was used to collect aggressive cells that invaded through Matrigel. We found that only about 1% of PANC-1 cells successfully invaded through the Matrigel. This percentage of INV is comparable to the number of cancer stem-like cells (CSC) that are speculated to be present within a population of cancer cell lines cultured *in vitro* [22]. To study whether INV have higher invasiveness compared to WCC, a re-invasion assay was performed (Supplemental Fig. 1). INV showed 2.24 ± 0.14 times higher invasiveness compared to WCC on Day 1 after collection from the undersurface of transwell membranes. The increased invasiveness of INV although not transient, was short lived and returned to the basal level by Day 11 (Fig. 1A). Therapy resistance being a hallmark of metastatic cells, we then examined the radio-sensitivity of INV and WCC by

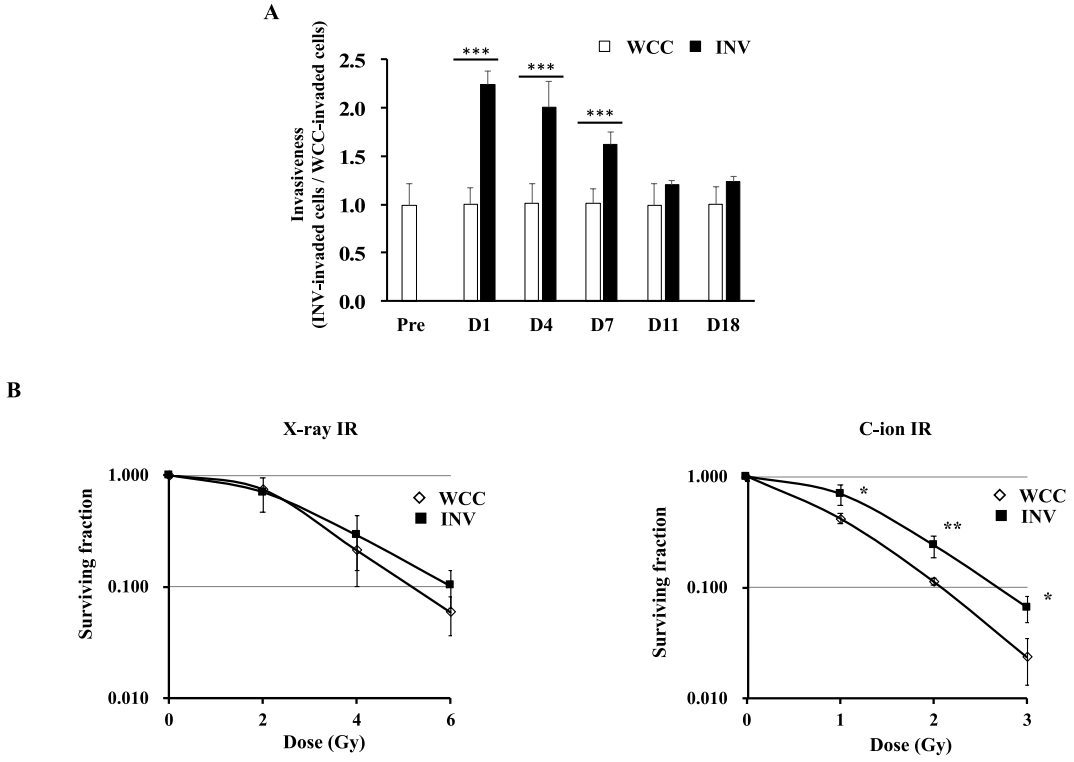

Fig. 1. Invaded pancreatic cancer cells were associated with increased invasiveness and resistance to C-ion radiation (A) Whole cultured PANC-1 cells (WCC) and INV collected from underneath of transwell membranes were used for invasion assay as shown in Supplemental Fig. 1. Number of invaded cells were counted, and ratio of invaded cells of INV group to WCC group was summarized in graph. Data are presented as mean ± SDs of triplicate samples. ***P $<$ 0.001. (B) Surviving fraction of X-ray- or C-ion-irradiated WCC or INV cells were shown in graph. Data are presented as mean ± SDs of triplicate samples. *P $<$ 0.05, **P $<$ 0.01.

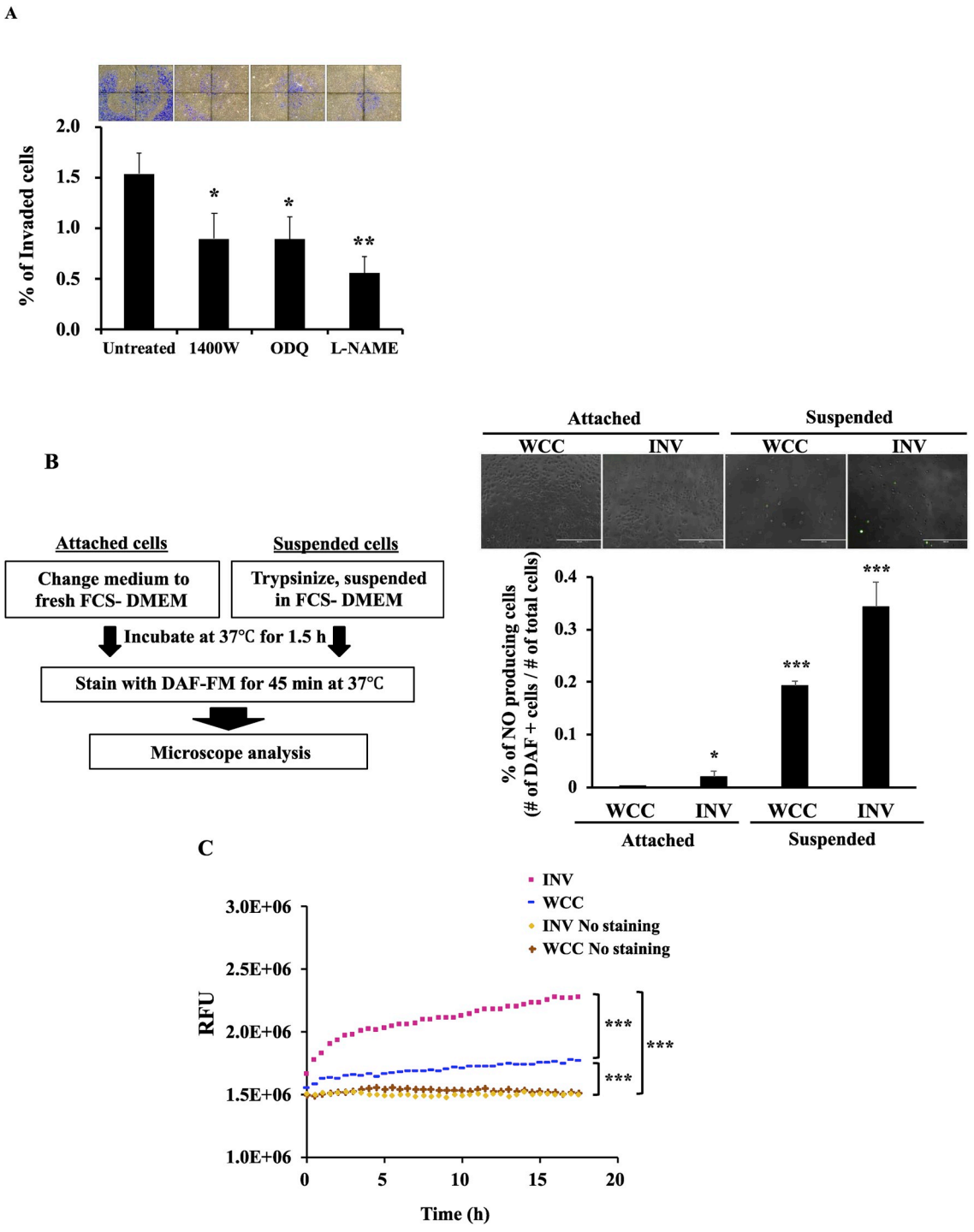

Fig. 2. Low flux of NO significantly induced PANC-1 invasion (A) Invasion assay was performed with using 1400W (20 μM), ODQ (1 μM), or L-NAME (500 μM). Percent of invaded cells were shown in graph. Data are presented as mean ± SDs of triplicate samples. *P < 0.05, ** < 0.01. (B) WCC or INV of either dish-adherent (attached) or suspended in serum free medium (suspended), were stained with DAF-FM, and visualized with fluorescent microscopy. Percent of DAF-positive cells were calculated as the number of DAF-positive cells divided by the number of total cells counted from bright field image (n = 3). *P < 0.05, ***P < 0.001. (C) Fluorescent signals of DAF-positive WCC or INV in suspended condition were measured with plate reader for 17 h. WCC: DAF-stained WCC, INV: DAF-stained INV, WCC No staining or INV No staining: WCC or INV without staining with DAF-FM, respectively (n = 3). ***P < 0.001. (D) DAF-FM fluorescent signals of 4 h-suspended INV were measured with plate reader, and compared to the signals of standard curve established with different concentrations of DETA/NO added into medium (n = 3). (E) Invasion assay was performed with using L-NAME (500 μM) with or without appropriate concentration of DETA/NO. Percent of invaded cells were shown in graph. Data are presented as mean ± SDs of triplicate samples. **P < 0.01, *** < 0.001 (F–H) NOS1, NOS2, NOS3 mRNA expressions were detected with using RT-PCR. Ratio of expression levels to those of attached-WCC FCS+ was calculated and shown in graph (n = 3). *P < 0.05, **P < 0.01, ***P < 0.001. Expression of phosphorylated NOS3 proteins were examined with Capillary western blot and bands were shown.

performing colony formation assay after X-ray or C-ion irradiation to assess if the invasive cells were also resistant to radio-therapy. While there were no observable differences in sensitivity of INV or WCC towards X-ray radiation, C-ion radiation induced a dose dependent decrease in survival of both WCC and INV, with INV showing significantly higher resistance to C-ion radiation compared to WCC (Fig. 1B). A comparison of surviving fraction between X-ray and C-ion RT showed that the dosage of X-ray required to elicit a similar response to C-ion RT was two to three times higher [23]. This data supports higher effectiveness of C-ion RT but at the same time suggests increased aggressiveness and higher resistance of INV. Thus, the use of focused irradiation for pancreatic cancer treatment may leave behind the recalcitrant cells with the INV phenotype which may subsequently lead to metastatic disease and relapse.

3.2. Low flux of NO significantly induces PANC-1 invasion

Previously, we have shown that the population of PANC-1 invading cells showed increased NO production upon C-ion radiation, and that a pan-NOS inhibitor, L-NMMA, was effective in reducing this invasion [15]. L-NMMA was also effective at decreasing the invasiveness of non-irradiated PANC-1 cells thereby indicating an involvement of NO in determining invasiveness of PANC-1 cells. To further elucidate which NOS isoform was involved in this abrogation of invasiveness, in the current study, we first inhibited NOS2 with the specific inhibitor, 1400W. 1400W showed a marginal but significant reduction in invasiveness of PANC-1, while L-NAME, a pan NOS inhibitor effectively suppressed invasion (Fig. 2A), suggesting that NO-induced invasiveness is tightly regulated and NOS2 along with other NOS isoforms may play a contributing role. The effect of NO can be dramatically different depending on their concentration, and low flux NO is known to activate soluble guanylyl cyclase (sGC) pathway [24]. Recently, NOS3, producing low flux NO, has been implicated in the pathogenesis of pancreatic ductal adenocarcinoma with development of invasive pancreatic lesions [25]. To further probe the role of NO-sGC pathway in our study, ODQ, a soluble guanylyl cyclase inhibitor was utilized that would inhibit effects downstream of NO-sGC pathway. Although the reduction level was not as effective as L-NAME, ODQ also significantly reduced invasiveness suggesting the importance of NO-sGC pathway in PANC-1 invasion. These results suggest that the flux of NO and the stage in the metastatic process at which NO is produced may determine invasiveness. To assess this *in vitro*, we next compared NO levels from INV and WCC cells in serum free medium, which is the same condition as the invasion assay. From the result, we found that 0.02% of all INV cells were DAF positive. This NO flux, although low, was significantly higher than DAF positive cells within the WCC, where only 0.001% of all WCC cells were DAF positive (Fig. 2B, Attached group). During invasion, cancer cells exhibit a series of adhesion/detachment events [26]. Detachment from ECM is observed as in the contractile machinery of amoeboid movement, as well as in the focal adhesion disassembly and detachment of the trailing edge observed in mesenchymal cell movement [27]. To address the effect of detachment from ECM on NO flux, the number of DAF-positive INV cells in suspension in serum-free medium for 1.5 h was compared to adherent cells, since cancer cells often form floating cell clusters when they are suspended in serum-free medium [28,29], and PANC-1 cells suspended in serum-free medium remain non-adherent and do not attach to the culture dish (Data not shown). Results from immunofluorescence staining showed that the number of DAF-positive cells in INV was 0.34% compared to 0.19% in WCC (Fig. 2B, Suspended group). While the fluorescent signal of DAF-positive cells increased in both

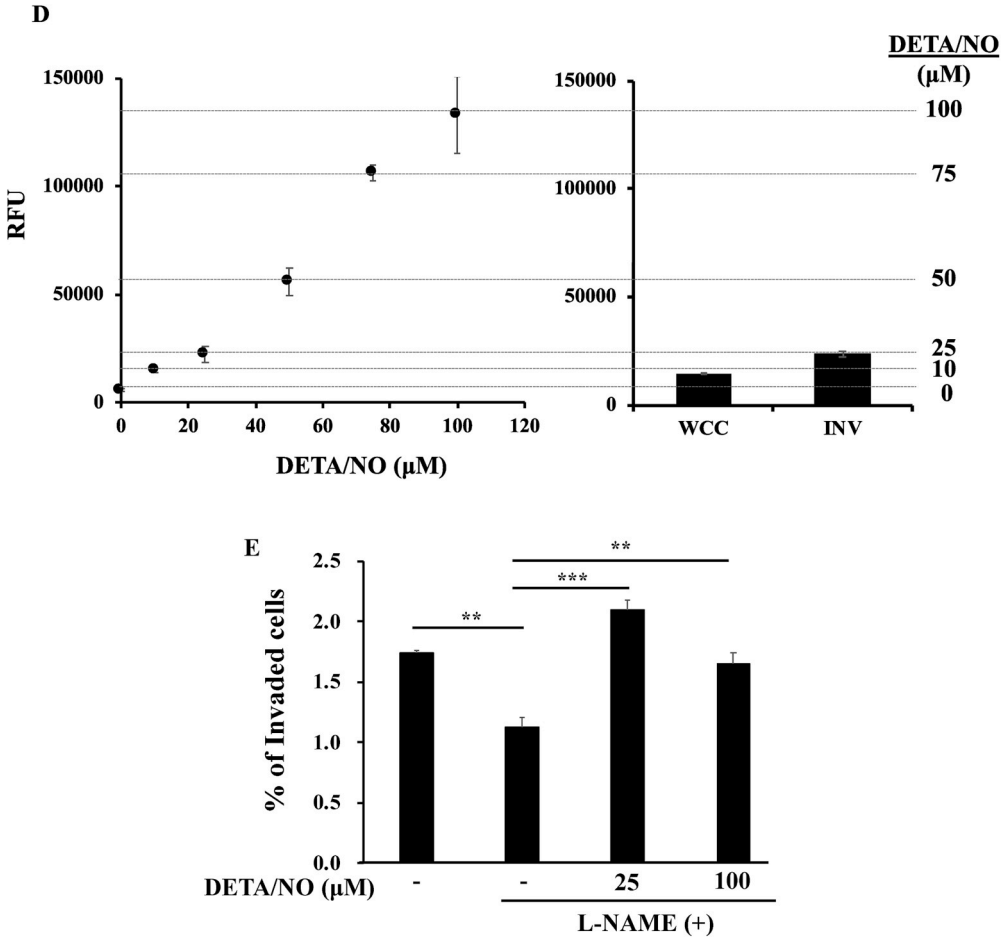

Fig. 2. (*continued*)

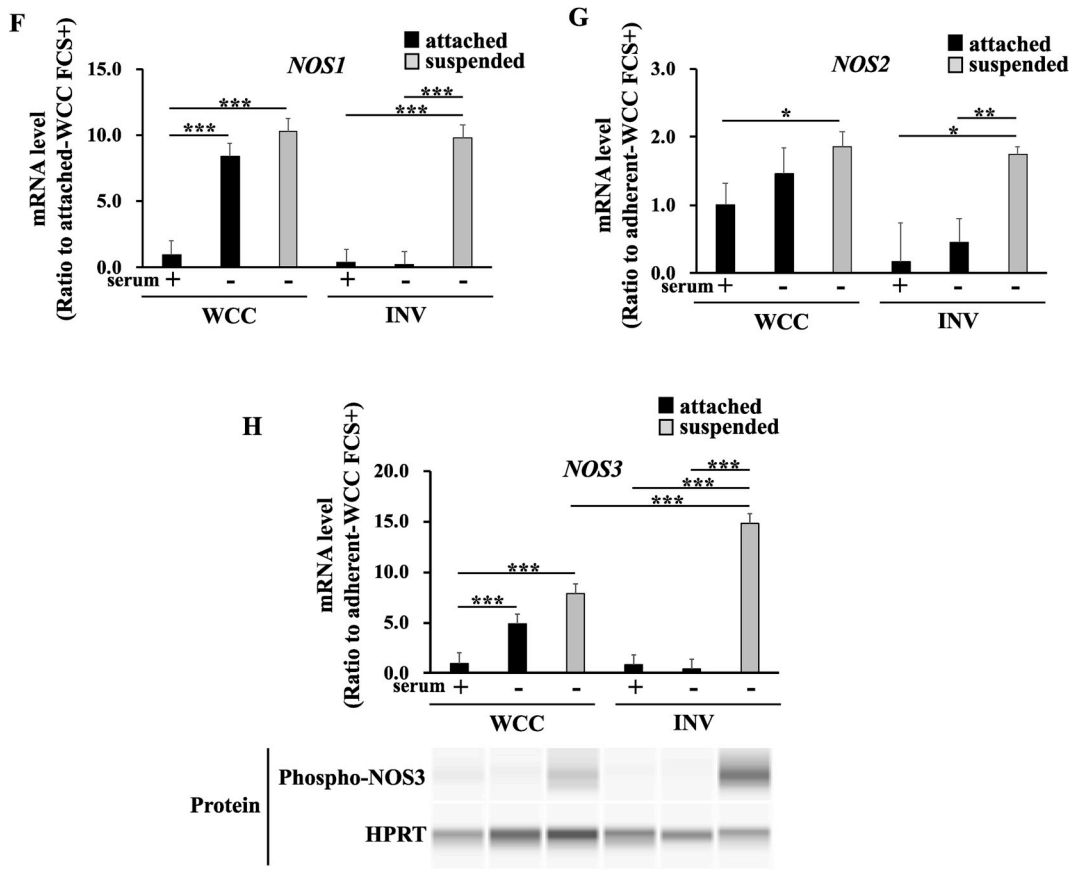

Fig. 2. (*continued*)

WCC and INV with prolonged suspension, these signals were significantly higher in INV (Fig. 2C). Furthermore, we used Griess assay and measured nitrite levels in the culture medium of WCC and INV, since cellular nitrite (NO_2^-) levels are historically measured to corroborate the presence of NO [30]. Consistent with Fig. 2C, suspension of INV in serum-free medium for 4 h produced 69.4 nM more nitrite than WCC, which was detectable after spiking both sets of samples with a known concentration of sodium nitrite in order to bring the nitrite levels within the detection limits of Griess assay. Our data thus show that the NO flux would be different at various stages of metastasis and that detachment from the ECM triggers a burst in NO production which in turn could facilitate the active invasive process.

It is well known that low NO concentrations promote cell survival, whereas high levels induce cell death [24,31–33]. Hence, next we attempted to elucidate the NO fluxes that determine cancer cell invasiveness *in vitro*. Using NO donors, such as DETA/NO, we can establish the specific concentration of NO and map the signaling pathways regulated at different NO levels; DETA/NO generates approximately a steady state NO flux in the nM range for the corresponding uM concentration of exogenous NO (ie., 1000 times lower flux) [31]. We have previously shown that at 3 h i.e.; conditions similar to those used in the current study, 100 μM DETA/NO in medium produces a NO flux of approximately 60 nM, measured by the Sievers Nitric Oxide Analyzer [34]. In addition, it has been shown that low concentrations of DETA/NO - about 25 μM–~100 μM that produces NO fluxes similar to the levels produced by NOS1 and NOS3, can effectively induce cell proliferation/survival, whereas NO produced by DETA/NO with higher than 100 μM–~500 μM (NOS2 level) induces anti-proliferative and apoptotic effects [31,33]. The fluorescent signal level produced with 4 h-suspended INV (INV_S) was found to be similar to those obtained with 25 μM DETA/NO (Fig. 2D), suggesting that NO levels observed in INV_S were in the range produced by NOS1 or NOS3, which has been identified as conducive to cell survival [24,31,33]. Concordantly, staining INV_S with DAF-FM and 7AAD (apoptosis marker) showed that DAF-positive cells were clearly distinct from the 7AAD-positive population (Supplemental Fig. 4). In addition, IncuCyte live cell imaging of DAF stained cells showed that DAF-positive cells did not take up PI and thus, NO-production was not associated with stress related to an onset of cell death pathways (Supplemental Fig. 5).

To further examine NO mediated regulation of invasiveness in the tumor micro-environment, the effect of exogenous NO on L-NAME inhibited PANC-1 invasion was studied. L-NAME treated PANC-1 showed reduced invasiveness compared to the non-treated cells, and addition of 25 μM DETA/NO restored the invasiveness of L-NAME-treated cells. The ability of NO to restore invasiveness reduced at higher concentration of 100 μM DETA/NO (Fig. 2E). Overall, these results suggest that low flux of NO plays a significant role in regulation and maintenance of cell survival and invasion in PANC-1 INVs.

Consistent with the low fluxes of NO, as expected, *NOS1* and *NOS3* were drastically upregulated in INV_S (Fig. 2F–H), whereas, in the case of WCC, treating cells simply with serum-free DMEM increased levels of *NOS1* and *NOS3* and these levels did not change significantly even when the cells were suspended for 4 h (WCC_S), suggesting that *NOS* is differentially regulated between INV and WCC. It is well known that the activation of NOS3 proteins are regulated by phosphorylation [35]. A comparison of phosphorylation of NOS3 protein in INV_S versus WCC_S showed a significant increase in p-NOS3 in INV_S (Fig. 2H), thereby suggesting a NOS3 mediated signaling in INV_S.

Furthermore, the number of DAF-positive INV cells drastically decreased with L-NAME treatment (Supplemental Fig. 6), thus L-NAME would be a good candidate diminishing NO production of INVs. Recently, the role of L-NAME has been implicated in survival of Kras mutation-positive non-small cell lung cancer [36]. Oncogenic mutation of *Kras* is common in most pancreatic tumors, and we have also

confirmed that PANC-1 that we used in this study has *Kras* mutation [37]. Thus, L-NAME may enhance the therapeutic benefits afforded by C-ion RT by multiple mechanisms.

3.3. Nitric Oxide Synthases induce expression of pro-metastatic genes in INV_S cells

To determine the possible role of NO in expression of pro-metastatic genes, levels of several pro-metastatic genes were analyzed with RT-PCR with or without L-NAME. The transcription of matrix metallopeptidase 9 (MMP9), the protease which degrades the ECM and hence paves the way for induction of metastatic spread [38], was increased in both WCC_S and INV_S, but the levels were much higher in INV_S (Fig. 3A). *S100A8* and *Lysyl oxidase (LOX)*, which play important roles in metastatic niche formation [39,40] were significantly upregulated in INV_S, compared to WCC_S (Fig. 3B and C). *CXCR4*, a chemokine receptor that is upregulated during metastasis [41], was also overexpressed in INV_S (Fig. 3D). L-NAME treatment significantly hampered the upregulation of *MMP9*, *S100A8, and CXCR4* in INV_S indicating that NO regulates the induction of these genes. Examination of *E-cadherin*, a transmembrane glycoprotein localized in adherent junctions and its loss is implicated in epithelial-mesenchymal transition (EMT) and cancer metastasis [42],

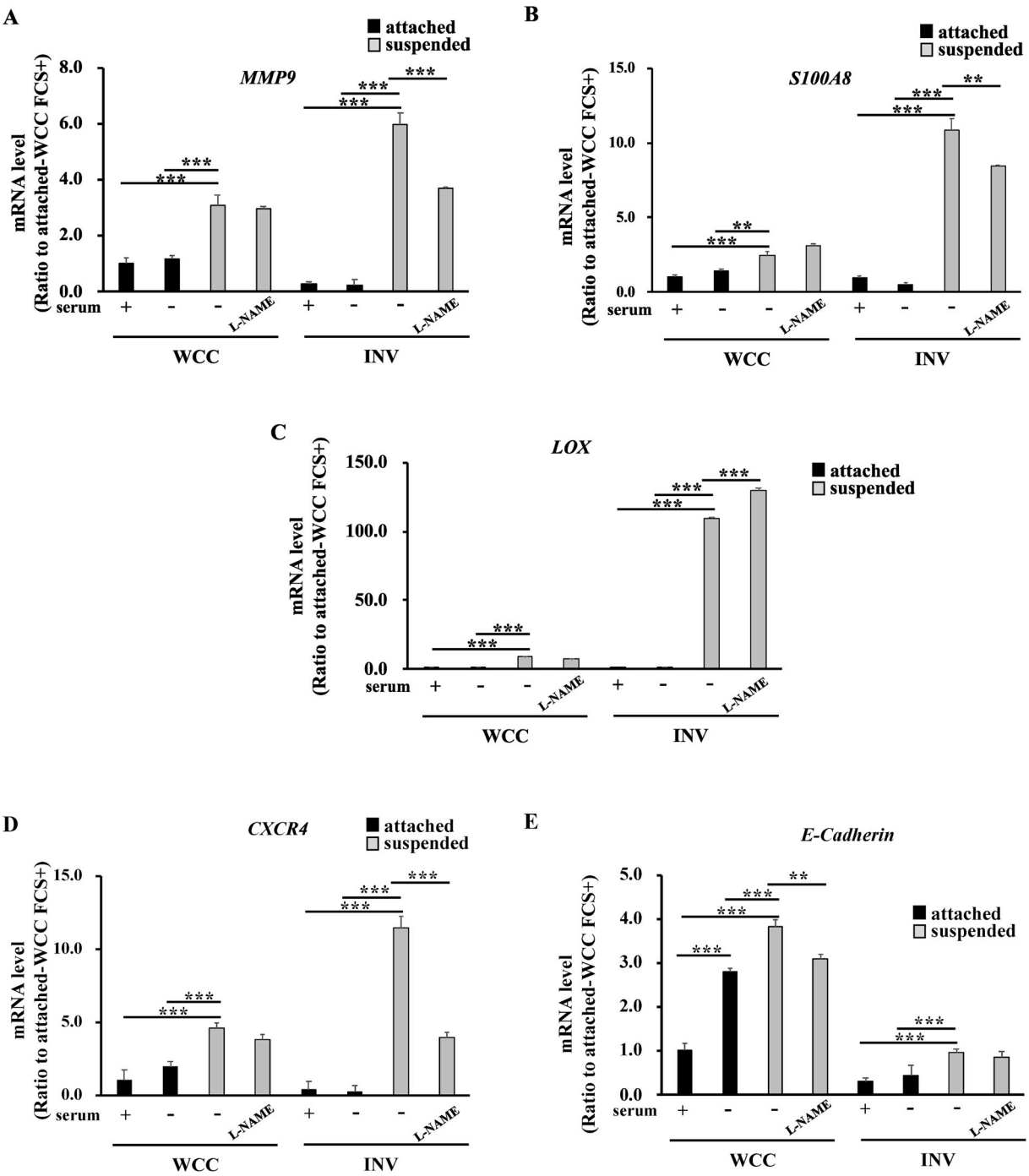

Fig. 3. Nitric Oxide Synthases induced expression of pro-metastatic genes in INVs cells Messenger RNA expressions of MMP-9 (A), S100A8 (B), LOX (C), CXCR4 (D), and E-Cadherin (E), were detected with RT-PCR. Ratio of expression levels over attached-WCC FCS + was calculated and shown in graph (n = 3). ** < 0.01, *** < 0.001.

showed low level of expression in INV, whereas WCC showed increased levels of *E-cadherin* in both attached or suspended condition (Fig. 3E). Overall, this data showed that INV are primed for metastasis as observed by higher induction of pro-metastatic genes in non-adherent condition with NO production by INV_S being the critical determinant leading to the induction of this highly metastatic, mesenchymal-like phenotype.

3.4. NO induces cancer stem cell-like phenotype in INV_S

To form a metastatic colony at a distant organ, cancer cells must survive and grow at the metastatic site [20], and stemness properties, such as self-renewal and tumorigenic properties, are important to form the metastatic colony [43]. The expression of stemness-related genes, *CD133, ALDH1, NANOG, SOX2* were all significantly enhanced in INV_S cells (Fig. 4A–D), indicating that non-adherent condition/detachment

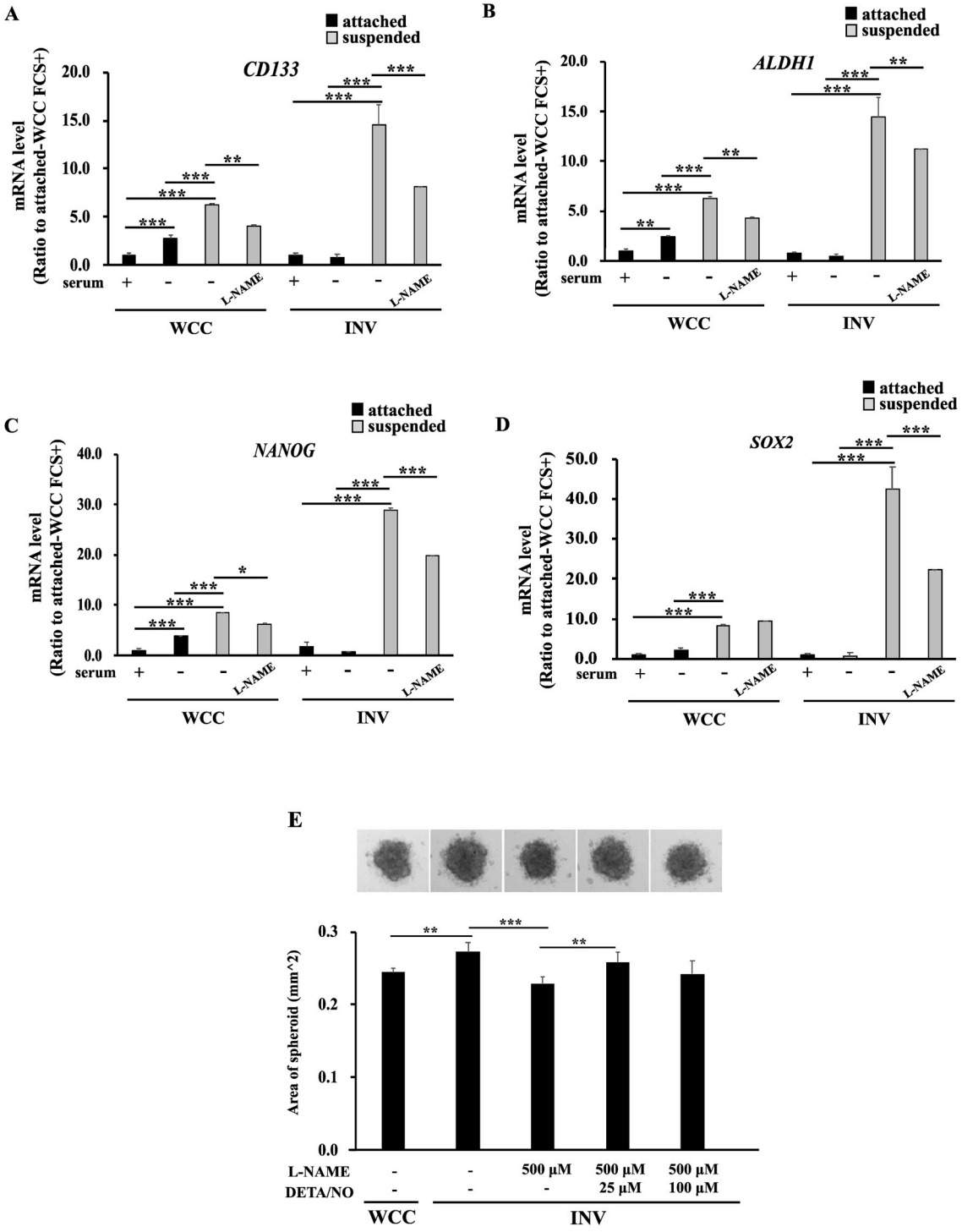

Fig. 4. NO induced cancer stem cell-like phenotype in INVs Messenger RNA expressions of CD133 (A), ALDH1 (B), NANOG (C), and SOX2 (D), were detected with RT-PCR. Ratio of expression levels to those of attached-WCC FCS+ was calculated and shown in graph (n = 3). *P < 0.05, ** < 0.01, *** < 0.001. (E) Spheroid formation assay in ultra-low attachment dish was performed with using WCC and INV. Spheroid area on Day 9 was measured and summarized in graph (n = 3). *P < 0.05, ** < 0.01, *** < 0.001. Representative spheroid image of each group was shown.

from ECM triggers the induction of these genes. The stemness-related genes in WCC_S were also upregulated but the levels were not as substantial as in INV_S (Fig. 4A–D). Furthermore, L-NAME was effective in reducing *CD133*, *ALDH1*, *NANOG* and *SOX2* inductions observed in INV_S, suggesting that NO plays a role in upregulating these genes in INV_S.

The ability of cells to form spheroids *in vitro* in defined, serum-free media is often used as the assay to confirm stem cell-like phenotype by assessing the self-renewal capability of cells. To confirm the stemness properties of INV, the spheroid formation ability of INV in ultra-low attachment dishes was examined. INV were collected from underneath the transwell membranes and were compared to the spheroid formation ability of WCC. The spheroid area on day 9 showed that INV formed significantly larger spheroids than WCC (Fig. 4E), and the higher ability of spheroid formation observed in INV was slightly but significantly reduced with L-NAME (Fig. 4E). The reduction of spheroid-genesis by L-NAME was restored upon addition of low dose DETA/NO (25 μM) whereas higher dose of DETA/NO (100 μM) had no significant effect on spheroid-genesis, suggesting that low flux of NO induces the increased spheroid-genesis as observed in INV. Although we observe that NO can regulate the expression of several 'stemness'-related genes, the exact mechanism involved in the regulation of spheroid formation ability must be investigated further.

3.5. MEK-ERK pathway is activated in INVs and has a role in PANC-1 invasion

Low flux of NO produced via NOS3 has been demonstrated to activate MEK-ERK and JAK-STAT pathways [44], and activation of these pathways is known to induce pro-metastatic and CSC-related genes [45–50]. NOS2 is also known to activate MEK-ERK and PI3K-AKT pathways [51], which can induce CSC related genes [45–47,51,52]. Thus, MEK-ERK, JAK-STAT and PI3-AKT pathways may be important in INV. We have previously reported that PI3K-AKT pathway was activated in PANC-1 INV compared to WCC, and PI3K inhibitors, LY294002 or Wortmannin, reduced PANC-1 invasion by over 40% [15]. To examine the role of MEK-ERK pathway in PANC-1 invasion, cells were treated with 0.5 nM or 10 nM, MEK inhibitor, U0126 or 1 nM or 10 nM, ERK inhibitor, ERK inhibitor 1. Inhibition of MEK-ERK pathway reduced PANC-1 invasion by 39% or 74%, respectively in the presence of 0.5 nM or 10 nM U0126, while 1 nM or 10 nM ERK inhibitor 1 blocked invasion by 40% or 48%, respectively (Fig. 5A). In contrast, JAK inhibitor, JAK inhibitor 1 at 0.1 μM or 5 μM, had no significant effect on blocking PANC-1 invasion (Fig. 5A), suggesting that PANC-1 invasiveness is mediated by MEK-ERK pathway, but not JAK pathway. The role of MEK-ERK and JAK-STAT pathway in cell survival is well established [53]. To verify that the reduced invasiveness is not a result of cell

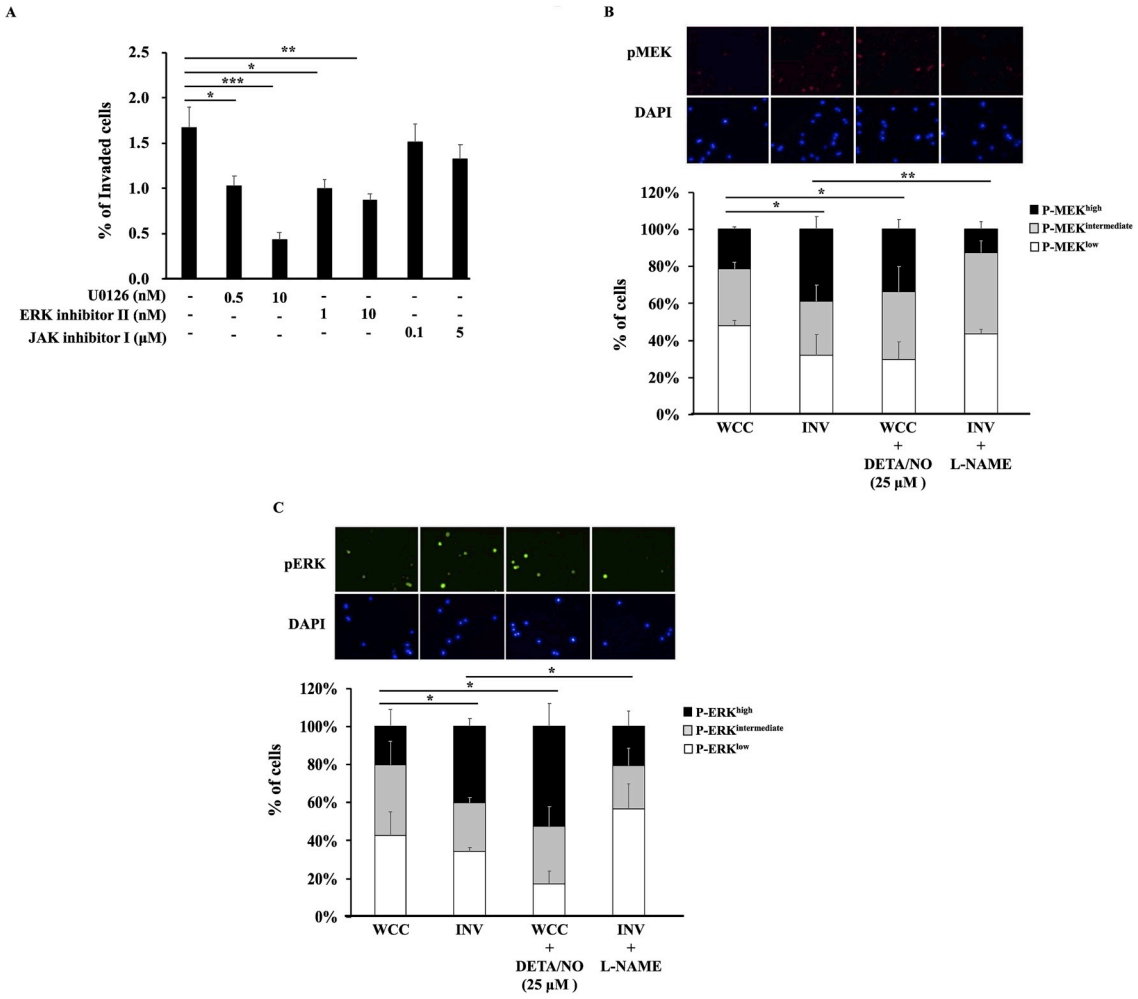

Fig. 5. MEK-ERK pathway was activated in INVs and had role in PANC-1 invasion (A) Invasion assay was performed with using U0126, ERK inhibitor II or JAK inhibitor I, and percent of invaded cells were shown in graph. Data are presented as mean ± SDs of triplicate samples. *P < 0.05, ** < 0.01, *** < 0.001. (B–C) WCC or INV suspended with serum-free medium with or without DETA/NO (25 μM) or L-NAME (500 μM) for 4 h were used for immunofluorescent study. (D–E) WCC suspended with serum-free medium with appropriate concentration of DETA/NO with or without 10 μM U0126 for 4 h were used for immunofluorescent study. Number of P-MEK^{high}, P-$MEK^{intermediate}$ or P-MEK^{low} (B, D) or P-ERK^{high}, P-$ERK^{intermediate}$ or P-ERK^{low} (C, E) were counted and percent of each populations were shown in graph. (n = 3). *P < 0.05, ** < 0.01. Representative image of each group was shown.

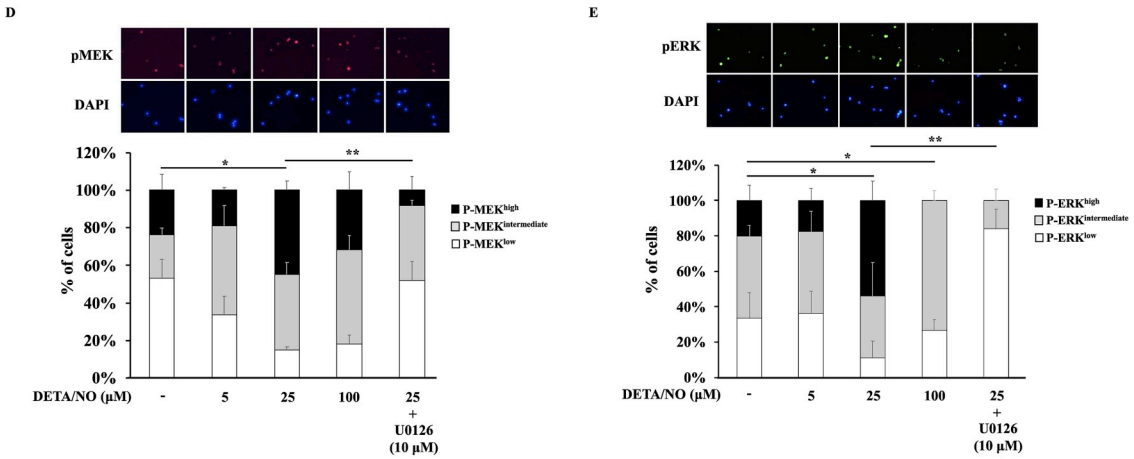

Fig. 5. (*continued*)

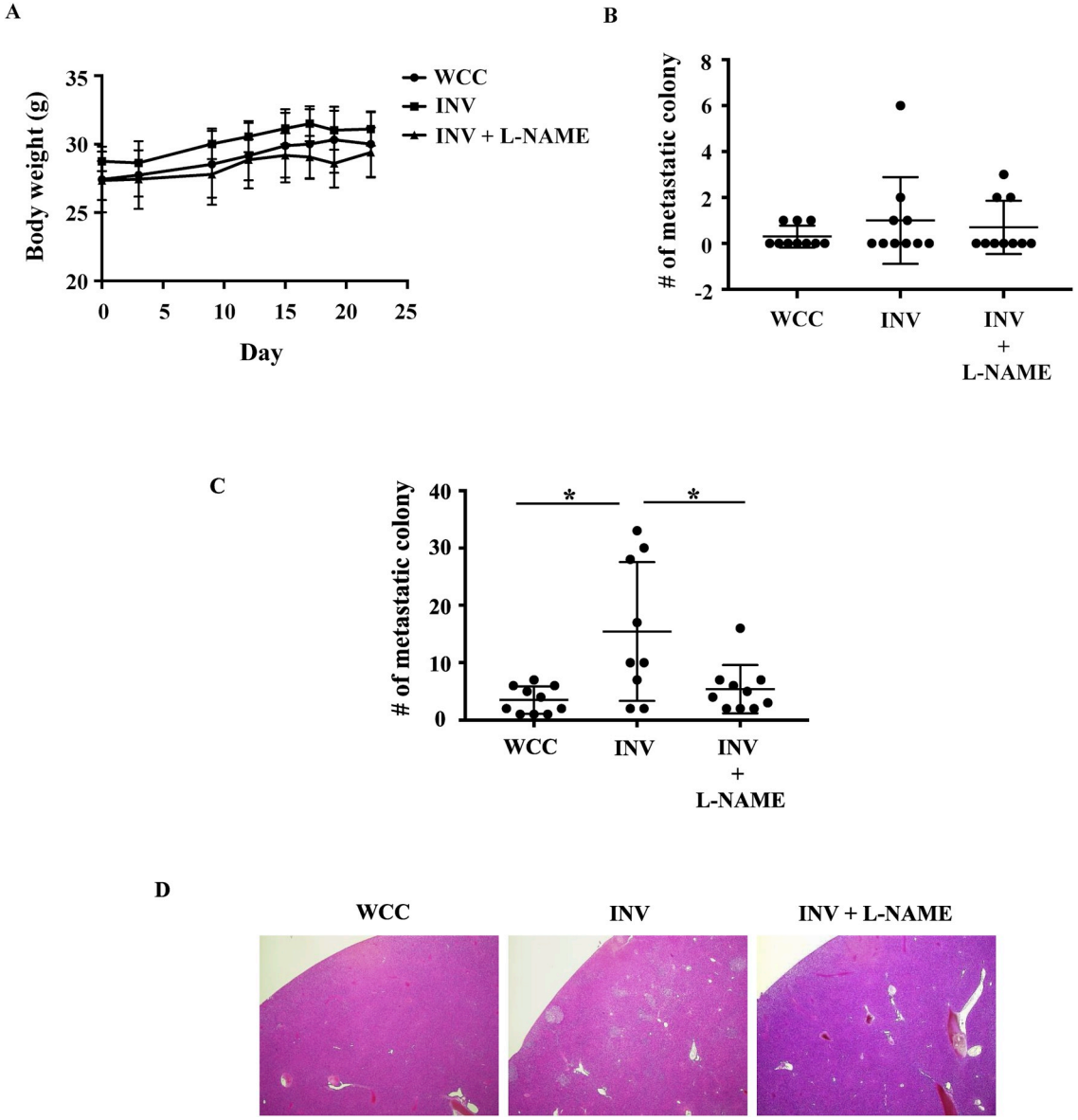

Fig. 6. Nitric oxide synthases mediated the *in vivo* metastatic spread of highly invasive INV (A) Mice body weights of WCC, INV or INV + L-NAME group were measured on alternate days, and summarized in graph (n = 10). (B) On day 25, lung and liver were harvested and fixed with Bouin's solution, and 48 h later, lung and liver were replaced with 70% ethanol. Number of metastatic colony of lung (B), or liver (C) was shown in graph. *P < 0.05 (D) Representative images of H&E-stained mouse liver sections were shown.

death, the effect of the inhibitors was examined on cell survival. Compared to control, U0126 (10 nM), ERK inhibitor 1 (10 nM), or JAK inhibitor 1 (5 μM) reduced cell survival by 15%, 9%, or 5%, respectively (Supplemental Fig. 7) while same concentrations of U0126 or ERK inhibitor 1 inhibited PANC-1 invasion by 74%, or 48% respectively (Fig. 5A). Thus, MEK-ERK pathway is involved in PANC-1 invasiveness.

To examine the difference in MEK-ERK activation in WCCs and INVs cells, we next stained WCCs and INVs with P-MEK or P-ERK antibody. As expected, INVs contains higher number of p-MEK^{high} or p-ERK^{high} cells compared to WCCs (Fig. 5B–C). Interestingly, number of p-MEK^{high} or p-ERK^{high} cells were increased with addition of 25 μM DETA/NO to WCC (Fig. 5B–C), whereas treatment of INV with L-NAME, reduced p-MEK^{high} or p-ERK^{high} population (Fig. 5B–C), indicating that number of p-MEK^{high} or p-ERK^{high} cells was regulated by specific NO flux. In addition, treating WCC with 25 μM DETA/NO, whose NO level is similar to those produced by INVs, significantly increased p-MEK^{high} or p-ERK^{high} cell numbers, whereas lower dose of DETA/NO, 5 μM, similar to the NO level that WCC produces, or higher dose of DETA/NO, 100 μM, has no significant effect or reduced effect on induction of p-MEK^{high} or p-ERK^{high} population (Fig. 5D–E). Furthermore, we confirmed that increased effect of 25 μM DETANO on p-MEK^{high} or p-ERK^{high} population was diminished with addition of MEK inhibitor, U0126 (Fig. 5D–E). Over all, these results suggest a NO flux-dependent induction of p-MEK^{high} or p-ERK^{high} population.

3.6. Nitric oxide synthases mediate the in vivo metastatic spread of highly invasive INV

So far, we found that suspension of INV in non-adherent conditions, in serum-free media triggers the induction of low level of NO production, which may have significant roles in the expression of several pro-metastatic and stemness-related genes. In addition, upregulation of many of these genes in INV$_S$ were reduced with L-NAME treatment. We used NSG mice to clarify whether INV have higher ability to metastasize *in vivo,* and if NO regulates this metastatic ability. Mice were injected with WCC (WCC group) or INV (INV group) into their spleen, and designated groups of animals were treated with L-NAME by administering L-NAME in the drinking water (INV + L-NAME group). Twenty-five days after injection, spleen, liver and lungs were harvested. There was no significant change in body weight between groups during the experiment (Fig. 6A). The average number of metastatic colonies in lung was less than 2 in all the groups, and there was no significant difference in lung metastasis between INV and WCC groups (Fig. 6B). In contrast, in the case of liver metastasis, INV group showed 14.4 ± 12 colonies compared to 3.5 ± 2.4 colonies for WCC group demonstrating significant increase in organ specific metastasis. These higher number of metastatic colonies in INV group were dramatically suppressed to 5.4 ± 4.2 colonies in the presence of L-NAME (Fig. 6C). Histometric analysis of H&E-stained mouse liver sections confirmed that INV did have higher ability to metastasize specially to liver in our model, and L-NAME was effective in reducing this metastatic ability (Fig. 6D).

4. Discussion

Cell invasion through ECM involves complex regulation of cell adhesion to and detachment from ECM proteins [26,27,54,55]. Specially, in the case of amoeboid movement, spherical cells lacking defined adhesions translocate by forming blebs or smooth membrane protrusions [27,56–58]. We had previously reported that PANC-1 forms a spherical shape to invade through Matrigel [11], indicating that PANC-1 INV uses amoeboid movement, lacking defined adhesions, for invasion. In this study, we find that detachment and suspension of PANC-1 INV *in vitro* in non-adherent conditions, induced NO production which in turn plays an important role in maintaining cell function in suspended cells, and detachment of normal, non-cancerous epithelial cells from ECM causes ATP depletion through reduced glucose uptake, and increased oxidative stress subsequently leading to anoikis, a form of programmed cell death [59]. Consistent with this idea, NO flux produced from INV$_S$ was low and within the range that is known to be effective in promoting cell survival, and flow cytometry data or real-time PCR analysis suggested that NO-producing cells were clearly distinct from the apoptotic cells. In addition, the fluxes of NO produced by INVs induced higher number of p-MEK^{high} or p-ERK^{high} cells, whose activation is known to increase cell survival [53]. Also, decreased adhesiveness with resistance to anoikis has been reported in circulating tumor cells in prostate cancer [60]. Thus, the ability of cells to produce low levels of NO under non-adherent conditions, such as fluxes produced by INV$_S$, may be one of the important factors aiding in successful survival in detached conditions and subsequent metastatic spread. Concordantly, INV showed higher metastasis in NSG mouse model.

Several stemness-related genes were upregulated in INV$_S$. Thus, INV$_S$ cells may harbor the CSC phenotype. However, expression of CD44, a CSC marker for pancreatic cancer [1], was not higher in INV compared to WCC (data not shown) and there were no differences in cell doubling time between INV and WCC. Thus, INV cells do not conform to the currently used description of a 'pancreatic CSC'. However, considering that the genetic background of INV and WCC are identical, it is intriguing that INV cell population, isolated from the identical parental cell line, PANC-1, exhibits such unique aggressive characteristics. Thus, it may be important to study the possible involvement of epigenetics in the regulation of INV, as we observed that higher invasiveness in re-invasion assay was transient and returned to basal level after culturing INV *in vitro* for 11 days.

The mesenchymal nature of INV$_S$ is further confirmed by the reduced E-cadherin expression [42] observed in INV compared to WCC. However, no reduction in expression was observed with L-NAME, suggesting that NOS may not be directly involved in EMT but in the later steps of the invasive process, indicated by the induction of CSC markers; MMP9, involved in initiating the extravasation from primary site [38]; CXCR4 [41]; as well as formation of the pre-metastatic niche by S100A8 [39]. LOX which is involved in the crosslinking of collagen and elastins to form the local ECM during the establishment of micrometastasis prior to the infiltration of the niche with tumor cells and myeloid cells [40], is independent of NOS. A recent paper reported that both NOS3 and NOS2 have roles in promoting CSC phenotype [61,62].

Interestingly, L-NAME effectively suppressed the upregulation of metastatic or CSC-related genes (Figs. 3 and 4), but single treatment with ODQ or 1400W had no significant effect on reducing these gene levels (data not shown). Concomitantly, L-NAME suppressed invasion, whereas 1400W or ODQ only slightly reduced invasiveness. Thus, NOS2 and NOS1 and/or NOS3 together induce metastatic and CSC property of INV, although there was no significant difference in NOS1 or NOS2 expression between WCC and INV, and only NOS3 expression and NOS3 phosphorylation were enhanced in INV. Previously, overexpression of NOS3 has been reported in pancreatic cancer which increases nitrosylation and activation of Ras [63,64]. In addition, NOS3, producing low flux NO, has been implicated in the pathogenesis of pancreatic ductal adenocarcinoma with development of invasive pancreatic lesions [25]. Low flux of NO that NOS1 or NOS3 produces is known to activate sGC pathway [31,33], and it appears that cGMP has a powerful role in the aggressive phenotype of certain cancers [65]. However, single treatment of ODQ, in this study, only slightly reduced invasiveness, suggesting that there are multiple mechanisms through which NO leads to increased PANC-1 invasion. Overall, our data showed that NOS2 and NOS1 and/or NOS3 together induce metastatic and CSC property of INV, and hence, NO plays important roles in several steps of metastasis leading to higher *in vivo* metastatic ability of INV cells compared to WCC in NSG mice.

We also treated WCC-injected mice with L-NAME. In the case of WCC bearing mice, L-NAME enhanced their metastasis (data not shown), indicating that blocking NO production in WCC may activate other signaling pathways or activate other cell populations that do not

produce NO, which enhances metastasis. We have not yet completely delineated the mechanisms of regulation of metastasis in WCC. In this context, flow cytometry data showed that there were only two kinds of populations in INV, which were either DAF-positive (NO-producing) cells or 7AAD-positive (apoptotic) cells, whereas, WCC exhibited a third population type, which did not take up DAF or 7AAD. It is possible that metastatic ability of DAF-negative 7AAD-negative population was activated with L-NAME (mechanism unknown), which caused the enhanced *in vivo* metastatic ability of WCC in presence of L-NAME. Since NO induction as well as pro-metastatic or stemness related genes were differently regulated in WCC, further studies will investigate how metastatic ability is regulated in WCC.

In a previous study, we used 31 cancer cell lines to examine whether C-ion radiation affects cancer cell invasiveness and found that C-ion radiation was effective to reduce invasion of many cell lines, but PANC-1 was the exception [37]. From the present study, it is indicative that the number of PANC-1 INV within the total number of PANC-1 cells may increase after C-ion radiation, because INV can survive better after C-ion radiation. L-NAME can effectively block the metastatic ability of such INV. Thus, L-NAME would be a promising candidate for use as an adjuvant for effective radiotherapy by blocking these radio-resistant and highly metastatic INV type of cells.

Acknowledgement

We are grateful to our colleagues from Cancer Stem Cell Team of the National Institute of Radiological Sciences Japan for providing expertise discussions that greatly assisted the research. We also thank Dr. Kenichiro Matsumoto, Ms. Megumi Ueno and Ms. Masayo Terada for helpful assistance to carry out our research smoothly. This study was performed in part by Research Project with Heavy Ions at the National Institute of Radiological Sciences Japan - Heavy Ion Medical Accelerator in Chiba (NIRS-HIMAC). This research was supported, in part, by the Intramural Research Program of the National Institutes of Health, USA. The content of this publication does not necessarily reflect the views or policies of the Department of Health and Human Services, nor does mention of trade names, commercial products, or organizations imply endorsement by the US Government. This work was supported, in part by Fund for the Promotion of Joint International Research (Grant No. 15KK0323 to MF), and Grant-in-Aid for Young Scientists (B) (grant no. 15K19833 to MF) from the Japan Society for the Promotion of Science.

Appendix A. Supplementary data

Supplementary data to this article can be found online at https://doi.org/10.1016/j.redox.2019.101158.

Disclosure statement

The authors declare that they have no competing financial interests.

References

[1] E. Giovannetti, C.L. van der Borden, A.E. Frampton, A. Ali, O. Firuzi, G.J. Peters, Never let it go: stopping key mechanisms underlying metastasis to fight pancreatic cancer, Semin. Canc. Biol. 44 (2017) 43–59.
[2] T.Y.S. Le Large, M.F. Bijlsma, G. Kazemier, H.W.M. van Laarhoven, E. Giovannetti, C.R. Jimenez, Key biological processes driving metastatic spread of pancreatic cancer as identified by multi-omics studies, Semin. Canc. Biol. 44 (2017) 153–169.
[3] P.J. Campbell, S. Yachida, L.J. Mudie, P.J. Stephens, E.D. Pleasance, L.A. Stebbings, L.A. Morsberger, C. Latimer, S. McLaren, M.L. Lin, D.J. McBride, I. Varela, S.A. Nik-Zainal, C. Leroy, M. Jia, A. Menzies, A.P. Butler, J.W. Teague, C.A. Griffin, J. Burton, H. Swerdlow, M.A. Quail, M.R. Stratton, C. Iacobuzio-Donahue, P.A. Futreal, The patterns and dynamics of genomic instability in metastatic pancreatic cancer, Nature 467 (2010) 1109–1113.
[4] F. van Zijl, G. Krupitza, W. Mikulits, Initial steps of metastasis: cell invasion and endothelial transmigration, Mutat. Res. 728 (2011) 23–34.
[5] O. Mohamad, B.J. Sishc, J. Saha, A. Pompos, A. Rahimi, M.D. Story, A.J. Davis, D.W.N. Kim, Carbon ion radiotherapy: a review of clinical experiences and preclinical research, with an emphasis on DNA damage/repair, Cancers (Basel) 9 (2017).
[6] M. Shinoto, S. Yamada, K. Terashima, S. Yasuda, Y. Shioyama, H. Honda, T. Kamada, H. Tsujii, H. Saisho, W.G.f.P. Cancer, Carbon ion radiation therapy with concurrent gemcitabine for patients with locally advanced pancreatic cancer, Int. J. Radiat. Oncol. Biol. Phys. 95 (2016) 498–504.
[7] S. Kawashiro, S. Yamada, M. Okamoto, T. Ohno, T. Nakano, M. Shinoto, Y. Shioyama, K. Nemoto, Y. Isozaki, H. Tsuji, T. Kamada, Multi-institutional study of carbon-ion radiotherapy for locally advanced pancreatic cancer: Japan carbon-ion radiation oncology study group (J-CROS) study 1403 pancreas, Int. J. Radiat. Oncol. Biol. Phys. 101 (2018) 1212–1221.
[8] ClinicalTrials.gov Identifier: NCT03403049.
[9] A. Malik, M. Sultana, A. Qazi, M.H. Qazi, G. Parveen, S. Waquar, A.B. Ashraf, M. Rasool, Role of natural radiosensitizers and cancer cell radioresistance: an update, Anal Cell Pathol. (Amst) 2016 (2016) 6146595.
[10] M. Fujita, Y. Otsuka, K. Imadome, S. Endo, S. Yamada, T. Imai, Carbon-ion radiation enhances migration ability and invasiveness of the pancreatic cancer cell, PANC-1, in vitro, Cancer Sci. 103 (2012) 677–683.
[11] M. Fujita, K. Imadome, T. Imai, Metabolic characterization of invaded cells of the pancreatic cancer cell line, PANC-1, Cancer Sci. 108 (2017) 961–971.
[12] C.R. Justus, N. Leffler, M. Ruiz-Echevarria, L.V. Yang, In vitro cell migration and invasion assays, J. Vis. Exp. 88 (2014) 51046.
[13] M. Lin, M.M. DiVito, S.D. Merajver, M. Boyanapalli, K.L. van Golen, Regulation of pancreatic cancer cell migration and invasion by RhoC GTPase and caveolin-1, Mol. Canc. 4 (2005) 21.
[14] A.J. Shirk, R. Kuver, Epidermal growth factor mediates detachment from and invasion through collagen I and Matrigel in Capan-1 pancreatic cancer cells, BMC Gastroenterol. 5 (2005) 12.
[15] M. Fujita, K. Imadome, S. Endo, Y. Shoji, S. Yamada, T. Imai, Nitric oxide increases the invasion of pancreatic cancer cells via activation of the PI3K-AKT and RhoA pathways after carbon ion irradiation, FEBS Lett. 588 (2014) 3240–3250.
[16] S. Endo, M. Fujita, S. Yamada, K. Imadome, F. Nakayama, T. Isozaki, T. Yasuda, T. Imai, H. Matsubara, Fra-1 enhances the radioresistance of colon cancer cells to X-ray or C-ion radiation, Oncol. Rep. 39 (2018) 1112–1118.
[17] T. Isozaki, M. Fujita, S. Yamada, K. Imadome, Y. Shoji, T. Yasuda, F. Nakayama, T. Imai, H. Matsubara, Effects of carbon ion irradiation and X-ray irradiation on the ubiquitylated protein accumulation, Int. J. Oncol. 49 (2016) 144–152.
[18] S.M. Namin, S. Nofallah, M.S. Joshi, K. Kavallieratos, N.M. Tsoukias, Kinetic analysis of DAF-FM activation by NO: toward calibration of a NO-sensitive fluorescent dye, Nitric Oxide 28 (2013) 39–46.
[19] V.M. Harris, Protein detection by simple Western™ analysis, Methods Mol. Biol. 1312 (2015) 465–468.
[20] E. Lonardo, M. Cioffi, P. Sancho, S. Crusz, C. Heeschen, Studying pancreatic cancer stem cell characteristics for developing new treatment strategies, J. Vis. Exp. (2015) e52801.
[21] L.A. Ridnour, R.Y. Cheng, J.M. Weiss, S. Kaur, D.R. Soto-Pantoja, D. Basudhar, J.L. Heinecke, C.A. Stewart, W. DeGraff, A.L. Sowers, A. Thetford, A.H. Kesarwala, D.D. Roberts, H.A. Young, J.B. Mitchell, G. Trinchieri, R.H. Wiltrout, D.A. Wink, NOS inhibition modulates immune polarization and improves radiation-induced tumor growth delay, Cancer Res. 75 (2015) 2788–2799.
[22] B. Bao, A. Ahmad, A.S. Azmi, S. Ali, F.H. Sarkar, Overview of cancer stem cells (CSCs) and mechanisms of their regulation: implications for cancer therapy (Chapter 14), Curr. Protoc. Pharmacol. (2013) Unit 14.25.
[23] T. Kamada, H. Tsujii, E.A. Blakely, J. Debus, W. De Neve, M. Durante, O. Jäkel, R. Mayer, R. Orecchia, R. Pötter, S. Vatnitsky, W.T. Chu, Carbon ion radiotherapy in Japan: an assessment of 20 years of clinical experience, Lancet Oncol. 16 (2015) e93–e100.
[24] D.D. Thomas, L.A. Ridnour, J.S. Isenberg, W. Flores-Santana, C.H. Switzer, S. Donzelli, P. Hussain, C. Vecoli, N. Paolocci, S. Ambs, C.A. Colton, C.C. Harris, D.D. Roberts, D.A. Wink, The chemical biology of nitric oxide: implications in cellular signaling, Free Radic. Biol. Med. 45 (2008) 18–31.
[25] B.L. Lampson, S.D. Kendall, B.B. Ancrile, M.M. Morrison, M.J. Shealy, K.S. Barrientos, M.S. Crowe, D.F. Kashatus, R.R. White, S.B. Gurley, D.M. Cardona, C.M. Counter, Targeting eNOS in pancreatic cancer, Cancer Res. 72 (2012) 4472–4482.
[26] G. Jacquemet, H. Hamidi, J. Ivaska, Filopodia in cell adhesion, 3D migration and cancer cell invasion, Curr. Opin. Cell Biol. 36 (2015) 23–31.
[27] P. Friedl, S. Alexander, Cancer invasion and the microenvironment: plasticity and reciprocity, Cell 147 (2011) 992–1009.
[28] S.K. Singh, I.D. Clarke, M. Terasaki, V.E. Bonn, C. Hawkins, J. Squire, P.B. Dirks, Identification of a cancer stem cell in human brain tumors, Cancer Res. 63 (2003) 5821–5828.
[29] D. Ponti, A. Costa, N. Zaffaroni, G. Pratesi, G. Petrangolini, D. Coradini, S. Pilotti, M.A. Pierotti, M.G. Daidone, Isolation and in vitro propagation of tumorigenic breast cancer cells with stem/progenitor cell properties, Cancer Res. 65 (2005) 5506–5511.
[30] E. Morcos, N.P. Wiklund, Nitrite and nitrate measurements in human urine by capillary electrophoresis, Methods Mol. Biol. 279 (2004) 21–34.
[31] L.J. Ignarro, Bruce A. Freeman, Nitric Oxide: Biology and Pathobiology, 3nd ed., Academic Press, 2017.
[32] D. Basudhar, V. Somasundaram, G.A. de Oliveira, A. Kesarwala, J.L. Heinecke, R.Y. Cheng, S.A. Glynn, S. Ambs, D.A. Wink, L.A. Ridnour, Nitric oxide synthase-2-derived nitric oxide drives multiple pathways of breast cancer progression, Antioxidants Redox Signal. 26 (2017) 1044–1058.
[33] V. Somasundaram, D. Basudhar, G. Bharadwaj, J.H. No, L.A. Ridnour, R.Y.S. Cheng,

M. Fujita, D.D. Thomas, S.K. Anderson, D.W. McVicar, D.A. Wink, Molecular Mechanisms of Nitric Oxide in Cancer Progression, Signal Transduction, and Metabolism, Antioxid Redox Signal, 2018 (Epub ahead of print).
[34] J.L. Heinecke, L.A. Ridnour, R.Y. Cheng, C.H. Switzer, M.M. Lizardo, C. Khanna, S.A. Glynn, S.P. Hussain, H.A. Young, S. Ambs, D.A. Wink, Tumor microenvironment-based feed-forward regulation of NOS2 in breast cancer progression, Proc. Natl. Acad. Sci. U. S. A. 111 (2014) 6323–6328.
[35] R.C. Kukreja, L. Xi, eNOS phosphorylation: a pivotal molecular switch in vasodilation and cardioprotection? J. Mol. Cell. Cardiol. 42 (2007) 280–282.
[36] N.L. Pershing, C.F.J. Yang, M. Xu, C.M. Counter, Treatment with the nitric oxide synthase inhibitor L-NAME provides a survival advantage in a mouse model of Kras mutation-positive, non-small cell lung cancer, Oncotarget 7 (2016) 42385–42392.
[37] M. Fujita, S. Yamada, T. Imai, Irradiation induces diverse changes in invasive potential in cancer cell lines, Semin. Canc. Biol. 35 (2015) 45–52.
[38] Y. Gao, Z. Guan, J. Chen, H. Xie, Z. Yang, J. Fan, X. Wang, L. Li, CXCL5/CXCR2 axis promotes bladder cancer cell migration and invasion by activating PI3K/AKT-induced upregulation of MMP2/MMP9, Int. J. Oncol. 47 (2015) 690–700.
[39] B. Psaila, D. Lyden, The metastatic niche: adapting the foreign soil, Nat. Rev. Canc. 9 (2009) 285–293.
[40] J.T. Erler, K.L. Bennewith, M. Nicolau, N. Dornhöfer, C. Kong, Q.T. Le, J.T. Chi, S.S. Jeffrey, A.J. Giaccia, Lysyl oxidase is essential for hypoxia-induced metastasis, Nature 440 (2006) 1222–1226.
[41] A. Müller, B. Homey, H. Soto, N. Ge, D. Catron, M.E. Buchanan, T. McClanahan, E. Murphy, W. Yuan, S.N. Wagner, J.L. Barrera, A. Mohar, E. Verástegui, A. Zlotnik, Involvement of chemokine receptors in breast cancer metastasis, Nature 410 (2001) 50–56.
[42] M. Canel, A. Serrels, M.C. Frame, V.G. Brunton, E-cadherin-integrin crosstalk in cancer invasion and metastasis, J. Cell Sci. 126 (2013) 393–401.
[43] K. Qureshi-Baig, P. Ullmann, S. Haan, E. Letellier, Tumor-Initiating Cells: a criTICal review of isolation approaches and new challenges in targeting strategies, Mol. Canc. 16 (2017) 40.
[44] R. Bolli, B. Dawn, Y.T. Xuan, Role of the JAK-STAT pathway in protection against myocardial ischemia/reperfusion injury, Trends Cardiovasc. Med. 13 (2003) 72–79.
[45] L.J. Xiao, P. Lin, F. Lin, X. Liu, W. Qin, H.F. Zou, L. Guo, W. Liu, S.J. Wang, X.G. Yu, ADAM17 targets MMP-2 and MMP-9 via EGFR-MEK-ERK pathway activation to promote prostate cancer cell invasion, Int. J. Oncol. 40 (2012) 1714–1724.
[46] S.Y. Lim, A.E. Yuzhalin, A.N. Gordon-Weeks, R.J. Muschel, Tumor-infiltrating monocytes/macrophages promote tumor invasion and migration by upregulating S100A8 and S100A9 expression in cancer cells, Oncogene 35 (2016) 5735–5745.
[47] X. Sun, L. Wei, Q. Chen, R.M. Terek, CXCR4/SDF1 mediate hypoxia induced chondrosarcoma cell invasion through ERK signaling and increased MMP1 expression, Mol. Canc. 9 (2010) 17.
[48] A. Ghosh, A. Pechota, D. Coleman, G.R. Upchurch, J.L. Eliason, Cigarette smoke-induced MMP2 and MMP9 secretion from aortic vascular smooth cells is mediated via the Jak/Stat pathway, Hum. Pathol. 46 (2015) 284–294.
[49] K. Hsu, Y.M. Chung, Y. Endoh, C.L. Geczy, TLR9 ligands induce S100A8 in macrophages via a STAT3-dependent pathway which requires IL-10 and PGE2, PLoS One 9 (2014) e103629.
[50] C. Ciccarelli, F. Vulcano, L. Milazzo, G.L. Gravina, F. Marampon, G. Macioce, A. Giampaolo, V. Tombolini, V. Di Paolo, H.J. Hassan, B.M. Zani, Key role of MEK/ERK pathway in sustaining tumorigenicity and in vitro radioresistance of embryonal rhabdomyosarcoma stem-like cell population, Mol. Canc. 15 (2016) 16.
[51] D. Basudhar, G. Bharadwaj, V. Somasundaram, R.Y.S. Cheng, L.A. Ridnour, M. Fujita, S.J. Lockett, S.K. Anderson, D.W. McVicar, D.A. Wink, Understanding the tumour microenvironment communication network from a NOS2/COX2 perspective, Br. J. Pharmacol. 176 (2019) 155–176.
[52] C.Y. Cheng, H.L. Hsieh, L.D. Hsiao, C.M. Yang, PI3-K/Akt/JNK/NF-κB is essential for MMP-9 expression and outgrowth in human limbal epithelial cells on intact amniotic membrane, Stem Cell Res. 9 (2012) 9–23.
[53] J.A. McCubrey, L.S. Steelman, S.L. Abrams, F.E. Bertrand, D.E. Ludwig, J. Becke, M. Libra, F. Stivala, M. Milella, A. Tafuri, P. Lunghi, A. Bonati, A.M. Martelli, Targeting survival cascades induced by activation of Ras/Raf/MEK/ERK, PI3K/PTEN/Akt/mTOR and Jak/STAT pathways for effective leukemia therapy, Leukemia 22 (2008) 708–722.
[54] E. Beerling, L. Ritsma, N. Vrisekoop, P.W. Derksen, J. van Rheenen, Intravital microscopy: new insights into metastasis of tumors, J. Cell Sci. 124 (2011) 299–310.
[55] P. Friedl, E.B. Bröcker, The biology of cell locomotion within three-dimensional extracellular matrix, Cell. Mol. Life Sci. 57 (2000) 41–64.
[56] A. Lorentzen, J. Bamber, A. Sadok, I. Elson-Schwab, C.J. Marshall, An ezrin-rich, rigid uropod-like structure directs movement of amoeboid blebbing cells, J. Cell Sci. 124 (2011) 1256–1267.
[57] E. Paluch, C. Sykes, J. Prost, M. Bornens, Dynamic modes of the cortical actomyosin gel during cell locomotion and division, Trends Cell Biol. 16 (2006) 5–10.
[58] R. Poincloux, O. Collin, F. Lizárraga, M. Romao, M. Debray, M. Piel, P. Chavrier, Contractility of the cell rear drives invasion of breast tumor cells in 3D Matrigel, Proc. Natl. Acad. Sci. U. S. A. 108 (2011) 1943–1948.
[59] T.R. Hurd, M. DeGennaro, R. Lehmann, Redox regulation of cell migration and adhesion, Trends Cell Biol. 22 (2012) 107–115.
[60] E.W. Howard, S.C. Leung, H.F. Yuen, C.W. Chua, D.T. Lee, K.W. Chan, X. Wang, Y.C. Wong, Decreased adhesiveness, resistance to anoikis and suppression of GRP94 are integral to the survival of circulating tumor cells in prostate cancer, Clin. Exp. Metastasis 25 (2008) 497–508.
[61] N. Charles, T. Ozawa, M. Squatrito, A.M. Bleau, C.W. Brennan, D. Hambardzumyan, E.C. Holland, Perivascular nitric oxide activates notch signaling and promotes stem-like character in PDGF-induced glioma cells, Cell Stem Cell 6 (2010) 141–152.
[62] C.E. Eyler, Q. Wu, K. Yan, J.M. MacSwords, D. Chandler-Militello, K.L. Misuraca, J.D. Lathia, M.T. Forrester, J. Lee, J.S. Stamler, S.A. Goldman, M. Bredel, R.E. McLendon, A.E. Sloan, A.B. Hjelmeland, J.N. Rich, Glioma stem cell proliferation and tumor growth are promoted by nitric oxide synthase-2, Cell 146 (2011) 53–66.
[63] A.K. Nussler, S. Gansauge, F. Gansauge, U. Fischer, U. Butzer, P.G. Kremsner, H.G. Beger, Overexpression of endothelium-derived nitric oxide synthase isoform 3 in the vasculature of human pancreatic tumor biopsies, Langenbeck's Arch. Surg. 383 (1998) 474–480.
[64] K.H. Lim, B.B. Ancrile, D.F. Kashatus, C.M. Counter, Tumour maintenance is mediated by eNOS, Nature 452 (2008) 646–649.
[65] R. Wang, Y. Li, A. Tsung, H. Huang, Q. Du, M. Yang, M. Deng, S. Xiong, X. Wang, L. Zhang, D.A. Geller, B. Cheng, T.R. Billiar, iNOS promotes CD24, Proc. Natl. Acad. Sci. U. S. A. 115 (2018) E10127–E10136.